SCIENTIFIC REPORTS
nature research

Check for updates

OPEN

Reconfigurable honeycomb metamaterial absorber having incident angular stability

Javad Shabanpour✉, Sina Beyraghi & Homayoon Oraizi

Ultrawide-angle electromagnetic wave absorbers with excellent mechanical properties are required in many diverse applications such as sensing, and stealth technologies. Here, a novel 3D reconfigurable metamaterial absorber (MMA) consisting of honeycomb and VO2 films is proposed. The proposed MMA exhibits a strong absorptivity above 90% in the widest incident angle up to 87° for TM- and TE polarized oblique incidences for THz wave propagating in yoz-plane. Under normal incidence, when VO2 films are in the insulating state, the proposed absorber exhibits high absorptivity in the frequency band of 1–4 THz. By increasing the temperature of the whole structure, the structural transformation of VO2 occurs and turns into the metallic phase. We have shown that under oblique incidence, the ohmic losses of VO2 films especially those parallel to the direction of the incident electric field are the most important absorption principles of the proposed MMA. Due to the ultra wide-angle absorption (angular stability) and mechanical performance, it is expected that the presented MMA may find potential applications, such as camouflage technologies, electromagnetic interference, imaging, and sensing. To the best knowledge of authors, the proposed MMA configuration exhibits the absorptivity in the widest incident angle ever reported.

Artificial metamaterials composed of subwavelength engineered scatterers have attracted massive attention owing to their abilities to modify the permittivity and permeability values to reach beyond those of composite materials found in nature, which may be structured for complex manipulation of electromagnetic (EM) waves[1–4]. The metamaterial absorbers (MMA), as an interesting application of metamaterials, have become a research hotspot in the past decade and have also been of great interest for solving electromagnetic interference problems, such as the stealth technologies, solar cells and sensor applications[5–8]. In 2008, Landy et al. introduced the first perfect MMA in which electric and magnetic resonances were generated in a narrow frequency band around 11.65 GHz[9]. MMAs have certain advantages compared with conventional absorbers[10–13] like ferrite[14] and Salisbury screen absorbers[15]. For instance, MMA can achieve a high level of absorptivity in spite of a thin substrate. Moreover, reconfigurable absorbers can be designed by tunable devices or materials[16,17]. Such great features made MMAs a promising candidate for various applications in the frequency spectrum, from microwaves to optical signals[18–21]. Since MMAs are made of periodic arrays of resonators, they can only realize efficient absorption in a narrow bandwidth. To solve this problem, several efforts have been made to broaden the absorption frequency band[22–24].

However, in all of the above strategies, the maximum absorption is obtained for the normal incidence and the absorption efficiency degrade for wider incidence angles. In general, the absorption characteristics of MMAs depend on the incident angle and wave polarization. The realization of polarization-independent MMAs is not difficult. It will be feasible for the symmetrical unit-cells placed in the vertical and horizontal directions[25,26]. On the other hand, the design of incident-angle-independent MMAs is a challenging task. Although several works have been attempted to address wide incident-angle MMAs, their maximum coverage of incident angle is limited to 70°[27–29]. In 2016, Shen et al., inspired by origami, found that the folded resistive patch array standing up on a metallic plate can exhibit a wide-angle absorbing characteristic up to 75° under the transverse magnetic (TM) polarization[30]. But for practical applications, besides possessing outstanding electromagnetic properties, wide-angle MMAs need to be strong enough and have excellent mechanical performance. Therefore, the above 3D absorber has poor mechanical properties which significantly hinders its further usage in real-world practical applications. On the other hand, recent research has revealed that structures with honeycomb cores have excellent mechanical performances and also can be used for electromagnetic wave absorption[31,32]. Based on such

Department of Electrical Engineering, Iran University of Science and Technology, Narmak, Tehran 16486-13114, Iran. ✉email: m.javadshabanpour1372@gmail.com

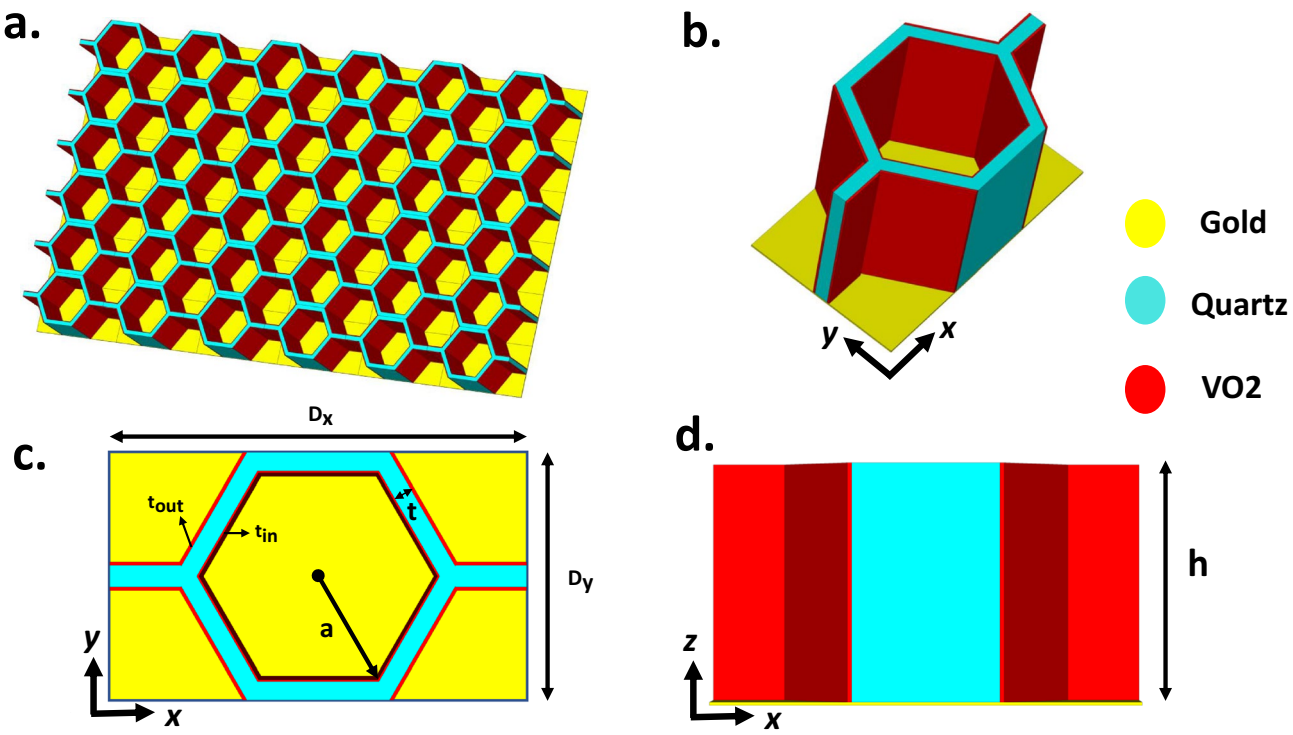

Figure 1. The structural design of the proposed RHA. (**a**) Perspective view. (**b**) Unit cell diagram. (**c**) Front view and (**d**) side view of the unit cell.

advantaged, we present a novel vanadium dioxide (VO2)-based honeycomb-like MMA which covers almost the full incident angle (0°–87°).

VO2 is a well-known smart material, which is known and utilized for its ultrafast and brutal reversible phase transition from insulator to metallic state above the critical temperature around $T_c = 340$ K[33]. This metal-insulator transition (MIT) due to the atomic level deformation in VO2 can be provoked by thermal[34], optical[35], or electrical stimuli[36]. MIT can occur within an order of several nanoseconds or even in picoseconds range for optical stimulation[37]. During MIT, the electrical conductivity has dramatic changes and can shift up to four orders of magnitude across the two phases[38]. Due to an ultrafast switching time, almost near room critical temperature and useful structural transition characteristics, VO2 has been identified as noteworthy material in reconfigurable metamaterial devices over a broad spectral range from GHz to optics. It has numerous practical applications at terahertz frequencies such as reprogrammable digital metasurfaces, THz waves modulator, and tunable antennas[39–41].

In this paper, a novel three-dimensional (3D) MMA is proposed, which consists of hexagonal honeycombs with VO2 thin films deposited on its walls as depicted in Fig. 1. The proposed absorber is engineered in such a way that it can retain the perfect absorptivity in a super-wide incident angle. In comparison to the class of wide-angle absorbers, our proposed MMA provides the widest coverage of incident angles, ever reported to the authors' knowledge. Since the design of the absorbers working under the oblique incident angles more than 75° has not yet been realized and reported due to its complexity, here for the first time, benefiting from VO2 exotic properties and tuning the proper electrical resistivity of VO2, we presented the MMA which can operate up to 87° for TM- and TE-polarized oblique incidences for THz waves propagating in a yoz-plane. To demonstrate the main mechanism of absorption, the induced electric field as well as the power loss density of the proposed Reconfigurable Honeycomb Absorber (RHA) are analyzed. We believe that the full coverage of incident-angle characteristics of the proposed RHA dramatically broadens the range of its applications in various fields such as imaging, sensing, and camouflage technology.

Results

Figure 1a,b shows the front view and top view of the proposed 3D RHA vertically mounted above a gold ground film. The periodicity of the proposed RHA unit-cells is $D_x = 68.62\,\mu$m and $D_y = 40.7\,\mu$m along the x and y directions, respectively.

The other geometrical parameters are $h = 38\,\mu$m, $a = 20\,\mu$m, $t = 3.5\,\mu$m, $t_{in} = 300$ nm and $t_{out} = 600$ nm, as shown in Fig. 1, respectively. The material of honeycomb is made of quartz with $\varepsilon_r = 3.75$ and $\tan\delta = 0.018$. The inner wall of the honeycomb in each unit of RHA is composed of 6 VO2 films that are joint together and the other 6 VO2 films are deposited on the outer walls of the honeycomb. The thickness of VO2 thin film on the inner and outer walls of the honeycomb are set to be 300 nm and 600 nm, respectively. The complex dielectric properties of the VO2 thin films can be defined by the Bruggeman effective-medium theory in the THz range,

where ε_d and ε_m indicate the dielectric constant of the insulator and metallic regions, respectively and V denotes the volume fraction of metallic regions[42].

$$\varepsilon_{VO_2} = \frac{1}{4}\{\varepsilon_d(2-3V) + \varepsilon_m(3V-1) + \sqrt{[\varepsilon_d(2-3V) + \varepsilon_m(3V-1)]^2 + 8\varepsilon_m\varepsilon_d}\} \quad (1)$$

At room temperature, the dielectric constant of VO2 thin film is about 9 in the insulting state[43] and by increasing the temperature of the structure through a resistive heater beneath the gold plate, the structural transformation occurs and VO2 turns into the metallic phase. VO2 films at THz frequencies display electrical conductivity in the range of $10 \sim 100$ S/m in the insulating state[43] and as high as an order of 5×10^5 S/m in the metallic state[44,45]. The bottom gold layer with the conductivity of $\sigma = 4.11 \times 10^7$ S/m plays an important role as a mirror in impeding the EM waves through the RHA. All the Full-wave EM simulations have been accomplished here by the commercial program CST Microwave Studio. For evaluating the reflection characteristics of the infinite array of RHA meta-atoms, the open boundary condition is applied along the z-axis, whilst periodic boundary conditions are also assigned along the x- and y-directions to incorporate the mutual coupling effect among the neighboring elements. Meanwhile, TE and TM polarized plane waves with different incidence angles were transmitted to the 3D RHA array along the z-axis.

Wave absorbing properties. For a metamaterial absorber, the absorptivity can be calculated by Eq. (2), where $A(\omega)$, $\Gamma(\omega)$ and $T(\omega)$ are the absorption, reflectance, and transmittance, respectively[46].

$$A(\omega) = 1 - \Gamma(\omega) - T(\omega) \quad (2)$$

Therefore, high absorptivity can be obtained by minimizing both the reflection and transmission coefficients. Since the gold plate thickness is much larger than the penetration depth of the incident wavefronts, $T(\omega)$ equals to zero and the absorptivity of the designed RHA can be simply computed by $A(\omega) = 1 - \Gamma(\omega)$. Under normal incidence, the reflection coefficient can be expressed as:

$$\Gamma(\omega) = \frac{Z(\omega) - Z_0}{Z(\omega) + Z_0} \quad (3)$$

where $Z(\omega)$ and Z_0 denotes the impedances of the RHA and free space, respectively. Equation (3) shows that the zero reflection condition is satisfied when $Z(\omega)$ and Z_0 are matched. Within the effective medium approximation, the impedance of a metamaterial can be controlled by tailoring the effective permittivity ε_r and the permeability μ_r as follows[47]:

$$Z(\omega) = \sqrt{\frac{\mu_0\mu_r(\omega)}{\varepsilon_0\varepsilon_r(\omega)}} \quad (4)$$

where ε_0 and μ_0 are the permittivity and permeability of the free space, respectively. By properly adjusting the VO2 electrical conductivity, the impedance of RHA can be matched to that of the free space. Therefore, the transmission coefficient can be minimized by dissipating the transmitted wave with significant VO2 ohmic losses at the intermediate temperatures. For the lowest and highest orders of electrical conductivity, VO2 is in the dielectric or metallic steady-state phases, respectively. On the other hand, the ohmic losses of the meta-atom are maximum at the intermediate temperatures which lead to a sharp drop in the reflection amplitude, so that the maximum absorption efficiency is attained in the entire frequency range of interest[40]. Therefore, in this condition, the loss factor of the RHA is high because of the large imaginary part of the refractive index (n).

Under the illumination of normal incident wave and considering the characteristics of VO2, numerical simulations have been performed by choosing the electrical conductivity of $\sigma = 8{,}000$ S/m. The simulated reflection and absorption spectra of the designed RHA for TE and TM polarized incident wave are depicted in Fig. 2a,d, respectively. The array has a near-unity absorbance in the frequency band of 1–4 THz. Note that for frequencies higher than 4 THz, the maximum periodicity of the structure exceeding one wavelength and the higher-order Floquet modes are generated. Consequently, the proposed structure exhibits a wideband absorptivity above 90% in 1.2–4 THz, leading to the fractional bandwidth as high as 108%. For a better insight, the induced electric field distribution, and the power loss density are demonstrated in Fig. 2b,c and Fig. 2e,f for both x- and y-polarizations at 2.5 THz, respectively. Observe that the VO2 films on the inner and outer walls of the honeycomb have stronger electric field density around them in comparison to the other RHA regions. Note that those VO2 films which are parallel to the incident electric field direction, are more excited. Furthermore, it can be concluded from Fig. 2, that the ohmic losses of VO2 films especially those parallel to the incident wave polarization are the most important absorption principles of the RHA. If the free-space–absorber impedance matching condition is well satisfied, a great portion of the incident THz wave energy can be effectively absorbed by the proposed 3D RHA. The normalized impedance (z) of the RHA can be calculated by[48]

$$z = \sqrt{\frac{(1+S_{11}^2)^2 - S_{21}^2}{(1-S_{11}^2)^2 - S_{21}^2}} = \frac{1+R}{1-R} \quad (5)$$

$$A = 1 - R = \frac{2}{z+1} = \frac{2[\mathrm{Re}(z)+1]}{[\mathrm{Re}(z)+1]^2 + \mathrm{Im}(z)^2} - i\frac{2\mathrm{Im}(z)}{[\mathrm{Re}(z)+1]^2 + \mathrm{Im}(z)^2} \quad (6)$$

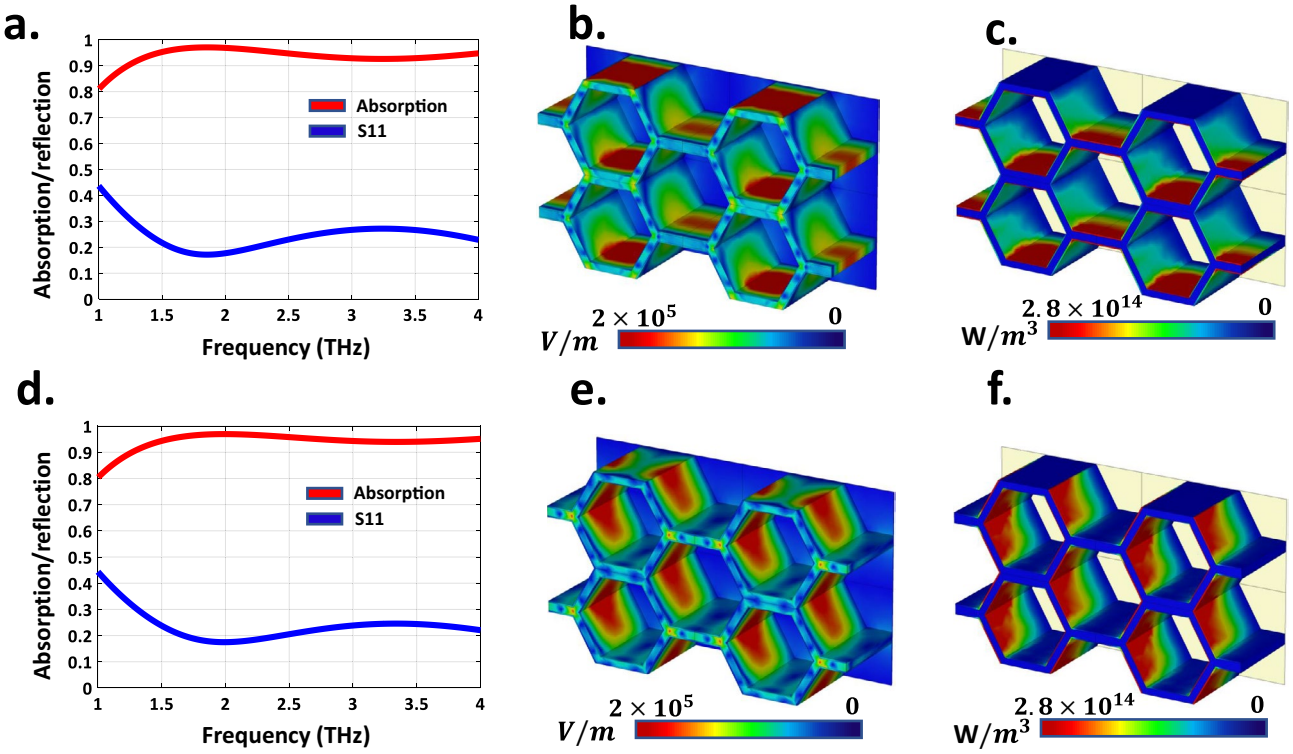

Figure 2. (**a**,**d**) Simulated results of absorptivity and reflectivity of the proposed RHA under the excitation of TM- and TE-polarized THz waves with normal incidences, respectively. (**b**,**e**) The electric field distributions on the unit cell at 2.5 THz under the excitation of x- and y-polarized THz waves with normal incidences, respectively. (**c**,**f**) The power loss distributions on the unit cell at 2.5 THz for x- and y-polarized THz waves with normal incidences.

The simulated normalized impedance of the proposed RHA is depicted in Fig. 3a. Observe that at resonance frequencies, the real part of the normalized impedance matches the free-space value $\mathrm{Re}(z) \approx 1$, and the imaginary part of the normalized impedance reaches zero simultaneously, $\mathrm{Im}(z) \approx 0$. Therefore, according to Fig. 3a, the principal mechanism of such a wideband absorption behavior of the RHA originates from the multiple resonance characteristics of the proposed structure.

When the incident angle increases, the deterioration of absorptivity is unavoidable since the zero-reflection condition differs under normal and oblique incidences. For example, at oblique incidence, the reflection coefficients for the perpendicular and parallel polarizations can be obtained by[49]:

$$\Gamma_{\perp}(\omega) = \frac{Z(\omega)\cos\theta_i - Z_0\cos\theta_t}{Z(\omega)\cos\theta_i + Z_0\cos\theta_t} \tag{7}$$

$$\Gamma_{\parallel}(\omega) = \frac{Z(\omega)\cos\theta_t - Z_0\cos\theta_i}{Z(\omega)\cos\theta_t + Z_0\cos\theta_i} \tag{8}$$

where θ_i and θ_t are the incident and transmission angles, respectively. Given that the absorptivity of MMAs changes when the incident angles are varied, so an angle-insensitive unit cell (having angular stability) must be designed for obtaining a full coverage incident angle MMA. We will show that our elaborately designed VO2 based unit cell is capable of realizing such a goal. Increasing the temperature of the whole structure enhances the electrical conductivity of VO2 thin films, and leads to near-unity absorption up to 87°.

Figure 3b–f demonstrates the absorption spectra of the RHA under different incident wave angles of TE- and TM-polarized waves propagating in the xoz-plane. Observe that benefiting from the structural transition of VO2 by increasing its temperature, our elaborately designed RHA can retain the absorptivity (by more than 90%) in a super-wide incident angle up to 87° for the TM-polarized wave. For the incident angles lower than 60°, VO2 should be in the insulator state (σ = 8,000 S/m), and for the incident angles greater than 60°, the structural transition in VO2 must occur to metal state ($\sigma = 5 \times 10^5$). S/m

According to Fig. 3, by increasing the incident angle, the absorbing bandwidth becomes narrow and the full coverage of incident angle of the proposed structure occurs at 1–1.3 THz. Besides, by increasing the temperature of the structure, the absorptivity of the TE-polarized oblique incidence drops sharply. To intuitively understand

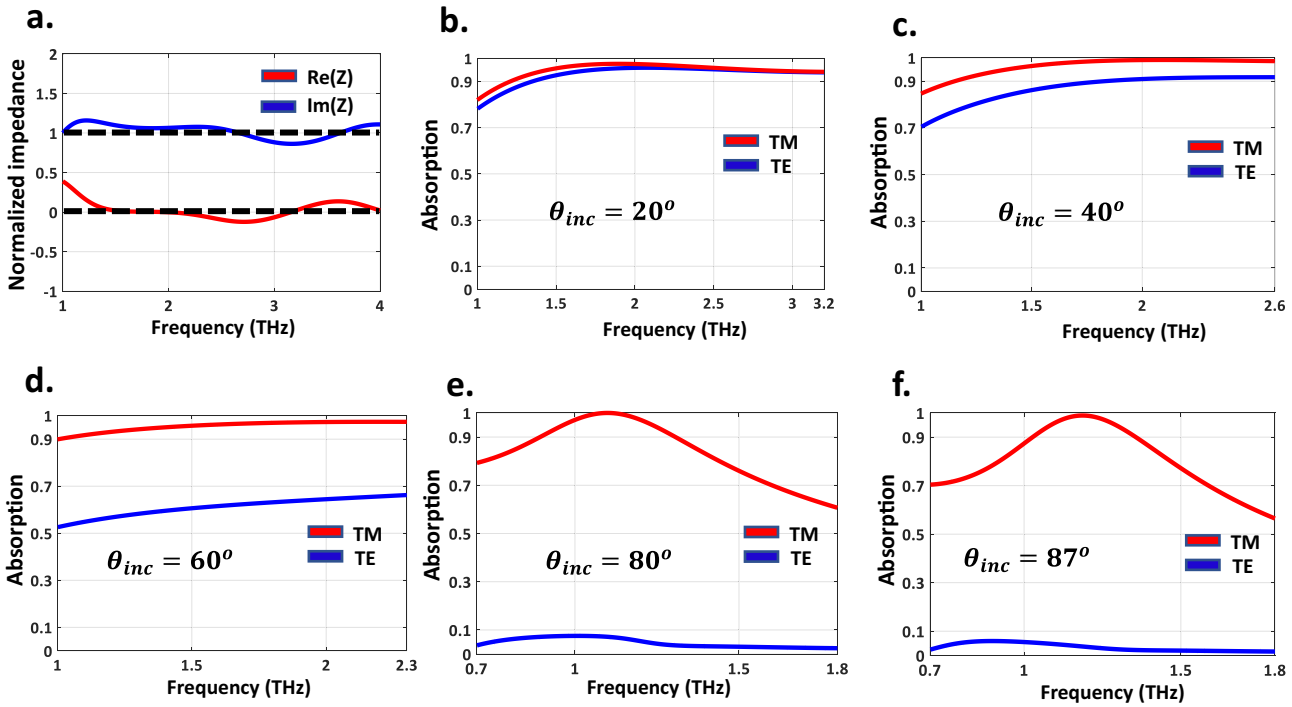

Figure 3. (**a**) The normalized impedance of the designed RHA versus frequency. The simulated absorption spectra for TE and TM polarization with the different incident angles of (**b**) 20°. (**c**) 40°. (**d**) 60°. (**e**) 80° and (**f**) 87°.

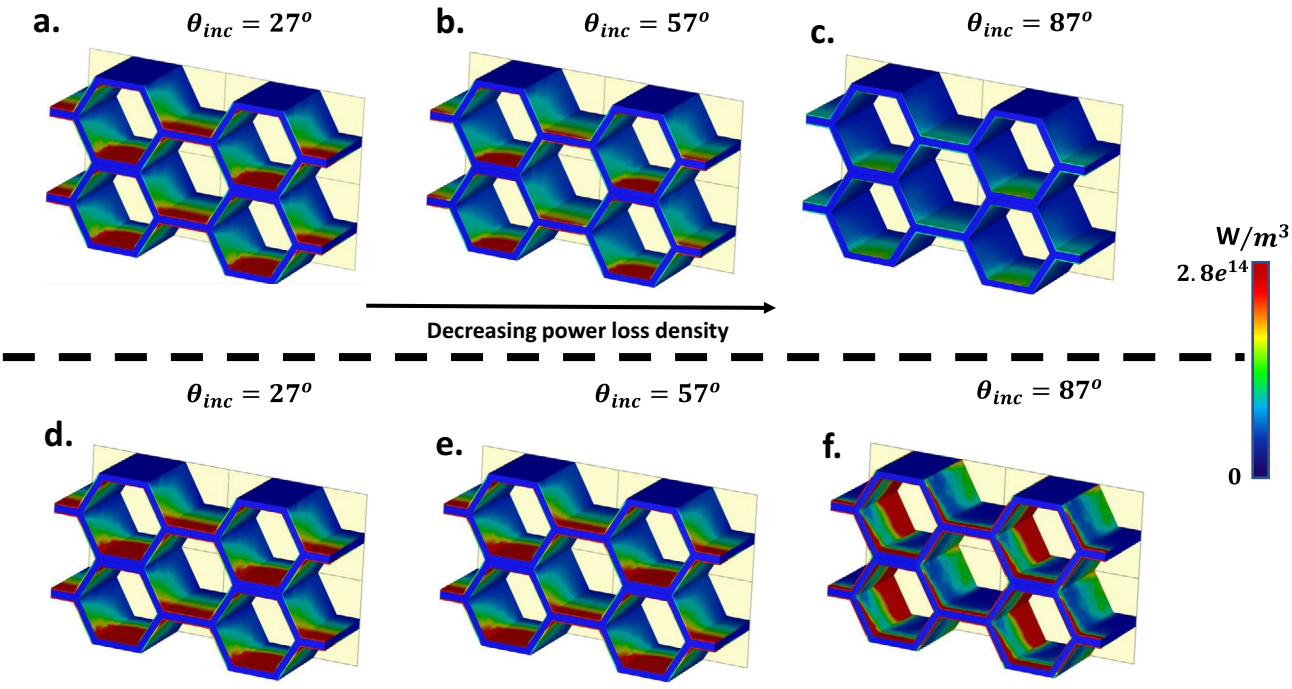

Figure 4. The power loss density distributions on the array at the various TM polarized incident angles of (**a**). 27°. (**b**) 57° and (**c**) 57° for electrical conductivity of 8,000 S/m at 1.3 THz. The power loss density distributions for electrical conductivity of VO2 (**d**) 8,000 S/m. (**e**) 12,000 S/m and (**f**) 5×10^5 S/m, respectively.

and interpret the absorption mechanism, the power loss density distributions of the proposed array at various angles are also depicted in Fig. 4. Observe that the power loss can be mostly attributed to the ohmic losses provided by VO2 thin films based on

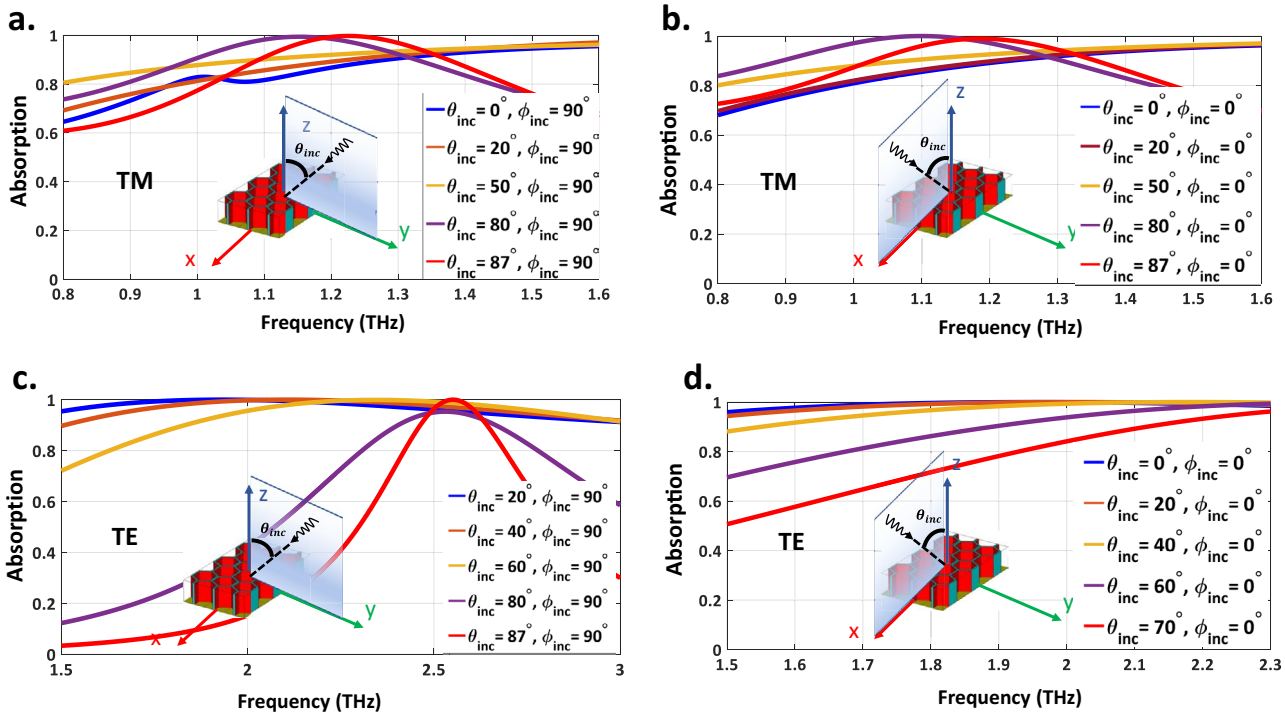

Figure 5. The simulated result of absorptivity for various situations of (**a**) THz waves propagating in yoz-plane with TM polarization. (**b**) THz waves propagating in xoz-plane with TM polarization. (**c**) THz waves propagating in yoz-plane with TE polarization. (**d**) THz waves propagating in xoz-plane with TE polarization.

$$P_{loss} = \int \sigma |E|^2 dv \tag{9}$$

whereby E is the tangent electric field. Figure 4 shows that the ohmic losses of VO2 films, especially those parallel to the direction of the incident electric field are the most effective factors of absorption of the proposed RHA.

Observe also from Fig. 4a–c that for a constant electrical conductivity, with the increase of oblique incident angle, the power loss density decreases. Equation (9) shows the only way to increase the power loss density is to increase the electrical conductivity of the films. As depicted in Fig. 4d–f, increasing the electrical conductivity of VO2 which can be dynamically tuned, plays an effective role in dissipating the incoming EM energy. Furthermore, when the oblique incident angle increases, the power loss distributes on the lateral sides of VO2 films instead of the upper and lower films.

Figure 5 shows the absorption spectra of the proposed RHA under different incident wave angles of TE- and TM-polarized waves in both xoz- and yoz-planes. For TM-polarized wave, as mentioned earlier, the near-unity absorption can be obtained up to 87° for the oblique incident wave propagating in the xoz- plane. Observe in Fig. 5b that this behavior also happens for THz waves propagating in the yoz-plane. We have mentioned in Fig. 3 that by increasing the temperature of the structure, the absorptivity of the TE-polarized oblique incidence drops sharply. But for different values of electrical conductivity of VO2 (see Fig. 5c), our elaborately designed structure can retain the absorptivity up to 87° for an oblique incident wave propagating in the yoz-plane. While for TE-polarized oblique incidence propagating in the xoz-plane, the effective permittivity of the RHA will gradually drop as long as the angle of incidence increases; therefore, the absorption peaks shift towards the higher frequencies (higher than 2.3 THz) where the higher-order Floquet modes are generated as can be observed from Fig. 5d. On the contrary, for the TM polarized wave, since the magnetic component of the incident wave is always perpendicular to the incidence plane at different incident angles, the anti-parallel currents are effectively excited, leading to an ultra-wide-angle absorption for TM-polarized oblique incidences for THz wave propagating in both xoz- and yoz-planes[50].

Discussion

In summary, we designed a novel reconfigurable metamaterial absorber that can support a good absorption for an almost complete incident angle range (having angular stability) by changing the electrical conductivity of the VO2 thin films placed onto the inner and outer walls of the honeycomb. For TM- and TE polarized oblique incidences for the THz wave propagating in the yoz-plane, the proposed RHA exhibits a strong absorptivity above 90% up to the incidence angle of 87°. Besides, the proposed configuration of the RHA consists of hexagonal honeycombs cores which have excellent mechanical performances. The ultra-wide-incident angle property (angular stability) of the RHA was justified through analyzing the induced electric field as well as the power loss density distributions. We have demonstrated that, by increasing the electrical conductivity of VO2 which can be dynamically tuned, the ohmic losses of VO2 films especially those parallel to the direction of incident electric

field are the most effective absorption factors of the proposed RHA. Furthermore, as the oblique incident angle increases, the power loss tend to distribute on the lateral sides of VO2 films instead of the upper and lower films. We believe that the proposed absorber may find great potential for engineering applications due to its angular stability and full incident angle absorption and mechanical performance.

Methods

In this section, we provide a brief introduction on the current fabrication technologies for fabricating the presented VO2-based honeycomb metamaterial absorber. This process can follow the steps below: the fabrication procedure begins with quartz honeycombs that are fabricated through 3D printing technology by means of the laser lithography method on the micrometer scale. 300 nm and 600 nm thick VO2 thin films are deposited on the outer and inner walls of the quartz honeycombs respectively; using magneton sputtered technique. Patterned VO2 thin films are annealed at 450 degrees Celsius. Then the 3D RHA with a total size of 68.62 μm $\times$ 40.7 μm can be obtained. All the full-wave numerical simulations are carried out by the means of CST Microwave Studio version 2016 (https://www.3ds.com/products-services/simulia/products/cst-studio-suite/).

Received: 14 July 2020; Accepted: 26 August 2020
Published online: 10 September 2020

References

1. Moeini, M. M., Oraizi, H., Amini, A. & Nayyeri, V. Wide-band beam-scanning by surface wave confinement on leaky wave holograms. *Sci. Rep.* **9**, 1–11 (2019).
2. Rajabalipanah, H., Abdolali, A., Shabanpour, J., Momeni, A. & Cheldavi, A. Asymmetric spatial power dividers using phase-amplitude metasurfaces driven by huygens principle. *ACS Omega.* **4**, 14340–14352 (2019).
3. Rajabalipanah, H., Abdolali, A., Shabanpour, J., Momeni, A. & Cheldavi, A. Addition theorem revisiting for phase/amplitude-encoded metasurfaces: Asymmetric spatial power dividers. arXiv:1901.04063**(arXiv preprint)** (2019).
4. Moeini, M. M., Oraizi, H. & Amini, A. Collimating cylindrical surface leaky waves for highly improved radiation characteristics of holograms. *Phys. Rev. Appl.* **11**, 044006 (2019).
5. Wang, B. X. Quad-band terahertz metamaterial absorber based on the combining of the dipole and quadrupole resonances of two SRRs. *IEEE J. Sel. Top. Quant.* **23**, 1–7 (2016).
6. Wang, B. X., Wang, G. Z. & Wang, L. L. Design of a novel dual-band terahertz metamaterial absorber. *Plasmonics* **11**, 523–530 (2016).
7. Wang, B. X., Wang, G. Z. & Sang, T. Simple design of novel triple-band terahertz metamaterial absorber for sensing application. *J. Phys. D Appl. Phys.* **49**, 165307 (2016).
8. Gholamian, M., Shabanpour, J. & Cheldavi, A. Highly sensitive quarter-mode spoof localized plasmonic resonator for dual-detection RF microfluidic chemical sensor. *J. Phys. D Appl. Phys.* **53**, 145401 (2020).
9. Landy, N. I., Sajuyigbe, S., Mock, J. J., Smith, D. R. & Padilla, W. J. Perfect metamaterial absorber. *Phys. Rev. Lett.* **100**, 207402 (2008).
10. Wang, B. X., Zhai, X., Wang, G. Z., Huang, W. Q. & Wang, L. L. A novel dual-band terahertz metamaterial absorber for a sensor application. *J. Appl. Phys.* **117**, 014504 (2015).
11. Wang, B. X. *et al.* Theoretical investigation of broadband and wide-angle terahertz metamaterial absorber. *IEEE Photon. Tech Lett.* **26**, 111–114 (2013).
12. Wang, B. X., Wang, G. Z., Wang, L. L. & Zhai, X. Design of a five-band terahertz absorber based on three nested split-ring resonators. *IEEE Photon. Tech Lett.* **28**, 307–310 (2015).
13. Wang, B. X., Xie, Q., Dong, G. & Huang, W. Q. Simplified design for broadband and polarization-insensitive terahertz metamaterial absorber. *IEEE Photon. Tech Lett.* **30**, 1115–1118 (2018).
14. Park, M. J., Choi, J. & Kim, S. S. Wide bandwidth pyramidal absorbers of granular ferrite and carbonyl iron powders. *IEEE Trans. Magn.* **36**, 3272–3274 (2000).
15. Fante, R. L. & McCormack, M. T. Reflection properties of the Salisbury screen. *IEEE Trans. Antennas Propag.* **36**, 1443–1454 (1988).
16. Martinez, I., Panaretos, A. H., Werner, D. H., Oliveri, G. & Massa, A. Ultra-thin reconfigurable electromagnetic metasurface absorbers. In *2013 7th European Conference on Antennas and Propagation (EuCAP)*. 1843–1847 (2013).
17. Song, Z. *et al.* Terahertz absorber with reconfigurable bandwidth based on isotropic vanadium dioxide metasurfaces. *IEEE Photon. J.* **11**, 1–7 (2019).
18. Wang, B. X., He, Y., Lou, P. & Xing, W. Design of a dual-band terahertz metamaterial absorber using two identical square patches for sensing application. *Nanosc. Adv.* **2**, 763–769 (2020).
19. Wang, B. X., He, Y., Lou, P., Huang, W. Q. & Pi, F. Penta-band terahertz light absorber using five localized resonance responses of three patterned resonators. *Results Phys.* **16**, 102930 (2020).
20. Wang, B. X., Tang, C., Niu, Q., He, Y. & Chen, T. Design of narrow discrete distances of dual-/triple-band terahertz metamaterial absorbers. *Nanosc. Res. Lett.* **14**, 1–7 (2019).
21. Wang, B. X., Wang, G. Z., Sang, T. & Wang, L. L. Six-band terahertz metamaterial absorber based on the combination of multiple-order responses of metallic patches in a dual-layer stacked resonance structure. *Sci. Rep.* **7**, 41373 (2017).
22. Nguyen, T. T. & Lim, S. Wide incidence angle-insensitive metamaterial absorber for both TE and TM polarization using eight-circular-sector. *Sci. Rep.* **7**, 1–11 (2017).
23. Bhattacharyya, S., Ghosh, S. & Vaibhav Srivastava, K. Triple band polarization-independent metamaterial absorber with bandwidth enhancement at X-band. *J. Appl. Phys.* **114**, 094514 (2013).
24. Lee, J., Yoo, M. & Lim, S. A study of ultra-thin single layer frequency selective surface microwave absorbers with three different bandwidths using double resonance. *IEEE Trans. Antennas Propag.* **63**, 221–230 (2014).
25. Lee, D. H., Ling, K., Lim, S. & Baek, C. W. Fabrication of polarization-insensitive, multi-resonant metamaterial absorber using wafer bonding of glass dielectric substrate. *Microelectron Eng.* **136**, 42–47 (2015).
26. Hu, F. *et al.* Design of a polarization insensitive multiband terahertz metamaterial absorber. *J. Phys. D Appl. Phys.* **46**, 195103 (2013).
27. Jiang, W. *et al.* Electromagnetic wave absorption and compressive behavior of a three-dimensional metamaterial absorber based on 3D printed honeycomb. *Sci. Rep.* **8**, 1–7 (2018).
28. Luo, M. *et al.* Broadband, wide-angle, and polarization-independent metamaterial absorber for the visible regime. *Opt. Express.* **25**, 16715–16724 (2017).
29. Bhattacharyya, S., Ghosh, S., Chaurasiya, D. & Srivastava, K. V. (A broadband wide angle metamaterial absorber for defense applications. In *2014 IEEE International Microwave and RF Conference (IMaRC)*. 33–36 (2014).

30. Shen, Y. *et al.* Origami-inspired metamaterial absorbers for improving the larger-incident angle absorption. *J. Phys. D Appl. Phys.* **48**, 445008 (2015).
31. Zhang, Q. *et al.* Bioinspired engineering of honeycomb structure-Using nature to inspire human innovation. *Prog. Mater. Sci.* **74**, 332–400 (2015).
32. Han, B. *et al.* Honeycomb-corrugation hybrid as a novel sandwich core for significantly enhanced compressive performance. *Mater. Des.* **93**, 271–282 (2016).
33. Song, Z. & Zhang, J. Achieving broadband absorption and polarization conversion with a vanadium dioxide metasurface in the same terahertz frequencies. *Opt. Express.* **28**, 12487–12497 (2020).
34. Hashemi, M. R. M., Yang, S. H., Wang, T., Sepúlveda, N. & Jarrahi, M. Electronically-controlled beam-steering through vanadium dioxide metasurfaces. *Sci. Rep.* **6**, 35439 (2016).
35. Coy, H., Cabrera, R., Sepúlveda, N. & Fernández, F. E. Optoelectronic and all-optical multiple memory states in vanadium dioxide. *J. Appl. Phys.* **108**, 113115 (2010).
36. Zimmers, A. *et al.* Role of thermal heating on the voltage induced insulator-metal transition in VO2. *Phys. Rev. Lett.* **110**, 056601 (2013).
37. Jeong, Y. G., Bahk, Y. M. & Kim, D. S. Dynamic terahertz plasmonics enabled by phase-change materials. *Adv. Opt. Mater.* **8**, 1900548 (2020).
38. Crunteanu, A. *et al.* Tunable THz metamaterials based on phase-changed materials (VO2) triggered by thermal and electrical stimuli. In *Terahertz, RF, Millimeter, and Submillimeter-Wave Technology and Applications X.International Society for Optics and Photonics*. Vol 10103, p. 101031H (2017).
39. Shabanpour, J. Programmable anisotropic digital metasurface for independent manipulation of dual-polarized THz waves based on a voltage-controlled phase transition of VO 2 microwires. *J. Mater. Chem.* **8**, 7189–7199 (2020).
40. Shabanpour, J., Beyraghi, S. & Cheldavi, A. Ultrafast reprogrammable multifunctional vanadium-dioxide-assisted metasurface for dynamic THz wavefront engineering. *Sci. Rep.* **10**, 1–14 (2020).
41. Shabanpour, J. Fully manipulate the power intensity pattern in a large space-time digital metasurface: From arbitrary multibeam generation to harmonic beam steering scheme. arXiv:2007.14051**(arXiv preprint)** (2020).
42. Zou, H., Xiao, Z., Li, W. & Li, C. Double-use linear polarization convertor using hybrid metamaterial based on VO2 phase transition in the terahertz region. *Appl. Phys. A-Mater.* **124**, 322 (2018).
43. Fan, F., Hou, Y., Jiang, Z. W., Wang, X. H. & Chang, S. J. Terahertz modulator based on insulator-metal transition in photonic crystal waveguide. *Appl. Opt.* **51**, 4589–4596 (2012).
44. Wang, D. *et al.* Switchable ultrathin quarter-wave plate in terahertz using active phase-change metasurface. *Sci. Rep.* **5**, 1–9 (2015).
45. Nouman, M. T. *et al.* Vanadium dioxide based frequency tunable metasurface filters for realizing reconfigurable terahertz optical phase and polarization control. *Opt. Express.* **26**, 12922–12929 (2018).
46. Lee, D., Hwang, J. G., Lim, D., Hara, T. & Lim, S. Incident angle-and polarization-insensitive metamaterial absorber using circular sectors. *Sci. Rep* **6**, 27155 (2016).
47. Landy, N. I. *et al.* Design, theory, and measurement of a polarization-insensitive absorber for terahertz imaging. *Phys. Rev. B Condens. Matter.* **79**, 125104 (2009).
48. Shen, X. *et al.* Polarization-independent wide-angle triple-band metamaterial absorber. *Opt. Express.* **19**, 9401–9407 (2011).
49. Wu, C. *et al.* Metamaterial-based integrated plasmonic absorber/emitter for solar thermo-photovoltaic systems. *Int. J. Opt.* **14**, 024005 (2012).
50. Fernández Álvarez, H., de Cos Gómez, M. E. & Las-Heras, F. A six-fold symmetric metamaterial absorber. *Materials* **8**, 1590–1603 (2015).

Author contributions

J.S. conceived the idea and designed the VO2-based meta-particle. S.B. conducted the simulations. Finally, J.S. wrote the manuscript based on the input from all authors. H.O. supervised the project and reviewed the manuscript.

Competing interests

The authors declare no competing interests.

Additional information

Correspondence and requests for materials should be addressed to J.S.

Reprints and permissions information is available at www.nature.com/reprints.

Publisher's note Springer Nature remains neutral with regard to jurisdictional claims in published maps and institutional affiliations.